American Mineralogist, Volume 85, pages 1416–1427, 2000

Mineralogy and magnetic behavior of pyrrhotite from a 260 °C section at the KTB drilling site, Germany

AGNES KONTNY,[1,*] HELGA DE WALL,[1] THOMAS G. SHARP,[2] AND MIHÁLY PÓSFAI[3]

[1]Geologisch-Paläontologisches Institut, Neuenheimer Feld 234, D-69118 Heidelberg, Germany
[2]Department of Geology, Arizona State University, Tempe, Arizona 85287-1404, U.S.A.
[3]Department of Earth and Environmental Sciences, University of Veszprém, Veszprém, POB 158, H-8201, Hungary

ABSTRACT

The ultradeep bore hole of the German Continental Deep Drilling Program (KTB) reached a depth of 9100 m and in situ temperatures of about 260 °C, offering an unique opportunity to study natural pyrrhotite. An integrative approach using optical methods, electron microprobe analysis, X-ray diffraction, transmission electron microscopy (see Pósfai et al. 2000), and temperature-dependent magnetic susceptibility measurements were used to characterize pyrrhotite types as a function of lithology and depth. We found a lithology-controlled distribution of pyrrhotite types to a depth of 8080 m, with ferrimagnetic, monoclinic 4C pyrrhotite (metal content 46.0 to 47.2 at%) as the dominant magnetic phase in gneisses and metabasic rocks. In the gneisses, a second pyrrhotite type with higher metal concentrations (46.9 to 48.2 at%) and antiferromagnetic behavior also occurs. At depths greater than 8080 m (in situ temperature > 230 °C) antiferromagnetic pyrrhotite, predominates in all lithologies. That 4C pyrrhotite does not occur below 8080 m, suggests that 4C is unstable above 230 °C in these rocks. Instead of 4C, a 5C type with a ferrimagnetic structure occurs below 8080 m. Thermomagnetic experiments indicate that the metal-poor Weiss-type pyrrhotite is stabilized by oxygen that causes the formation of magnetite during heating. From our observations on natural pyrrhotites we suggest that the magnetic λ-transition is related to the growth of ordered nA pyrrhotite domains to single domain size.

INTRODUCTION

Pyrrhotite ($Fe_{1-x}S$) is a common iron-sulfide mineral and an important constituent of ore deposits. The ferrimagnetic variety is a significant magnetic mineral in different rock types of the Earth's upper crust (Rochette et al. 1990; Pucher 1994). However, the mineralogic and magnetic phase relations in the Fe-S system are not fully understood, despite much experimental effort. The KTB deep drilling provides a natural laboratory for the investigation of pyrrhotite stability, magnetic properties, and the relations between structure and magnetic properties below 300 °C.

The KTB drilling site is located in the Oberpfalz region of eastern Bavaria, at the western margin of the largest Variscan basement complex in Central Europe, the Bohemian Massif. This region is also within the Erbendorf magnetic anomaly, an intensively studied region with a magnetic field reaching 120 nT (Pucher and Wonik 1990; Pucher 1994; Bosum et al. 1997, and references therein). Pyrrhotite occurs throughout most of the KTB profile and is the main carrier of magnetization. The KTB project consists of two boreholes drilled into medium-grade metamorphic rocks. The pilot hole (KTB VB) reached a depth of 4 km and the main hole (KTB HB) 9.1 km, corresponding to actual temperatures of about 120 and 260 °C, respectively (Emmermann and Lauterjung 1997).

* E-mail: agnes.kontny@urz.uni-heidelberg.de

The mineralogic and magnetic character of pyrrhotite depends on the crystal structure, which is based on the hexagonal close-packed NiAs structure. The nonstoichiometry of pyrrhotite is caused by a deficiency of iron atoms in the Fe-layers. As a function of composition and temperature, ordering of iron vacancies produces several superstructures of the hexagonal NiAs-type subcell, with a range of magnetic properties (Nakazawa and Morimoto 1971; Schwarz and Vaughan 1972; see also Table 1 in Pósfai et al. 2000). In general, two groups of pyrrhotite occur: (1) metal-poor pyrrhotite with a composition around Fe_7S_8 and a monoclinic structure (4C type); and (2) metal-rich pyrrhotites with compositions between Fe_9S_{10} and $Fe_{11}S_{12}$ and with pseudohexagonal structures (see the companion paper of Pósfai et al. 2000). Although Mössbauer studies do not reveal the presence of Fe^{3+} in the pyrrhotite structure (e.g., Vaughan and Craig 1979), the vacancy ordering model of Bertraut (1953), which has been confirmed by numerous structural refinements (e.g., Tokonami et al. 1972), depends on a formal valence scheme of the type $Fe_5^{2+}Fe_2^{3+}S_8$ and the Fe_9S_{10} type also needs Fe^{3+} for a charge balance. The lack of Mössbauer evidence for Fe^{3+} is explained by electron hopping (e.g., Ericsson et al. 1997).

The 4C type has strong ferrimagnetic behavior and magnetocrystalline anisotropy due to alternating vacancy-bearing and filled metal layers along **c**. Based on its ferrimagnetism, 4C pyrrhotite is also called Weiss-type and has Curie temperatures (T_c) between 310 and 325 °C (Schwarz and Vaughan 1972;

Li and Franzen 1996, and references therein). The metal-rich types show antiferromagnetic behavior up to the so-called λ-transition at about 200–220 °C, where they become ferrimagnetic (Rochette et al. 1990). Based on a sharp peak in the thermomagnetic curve at the λ-transition ($T\lambda$), metal-rich pyrrhotite is commonly called λ-type pyrrhotite. According to Schwarz and Vaughan (1972), the temperature of the λ-transition depends on composition and varies between 150 and 210 °C. The Curie temperatures of these pyrrhotites are between 265 and 295 °C (Rochette et al. 1990). The complex relationships among composition, structure type, and magnetic properties have not been previously investigated as a function of temperature and lithology in natural samples.

Ferrimagnetic 4C type is unstable at high temperatures, but the upper stability limit is uncertain. In dry experiments, the temperature at which synthetic monoclinic (4C) pyrrhotite transforms to a disordered superstructure ranges from 290 °C (Yund and Hall 1969) to 315 °C (Carpenter and Desborough 1964). In hydrothermal experiments, however, the upper stability limit of 4C pyrrhotite ranges from 254 °C (Kissin 1974) to 280 °C (Bennett and Graham 1980). On the other hand, the upper stability limit of natural monoclinic pyrrhotite appears to be about 225 °C (Kullerud 1986). The apparent upper-stability limit of 4C in experimental studies is determined by reaction kinetics (Kissin and Scott 1982), where the presence of water may enhance the transformation rate. Graham (1987) proposed that monoclinic pyrrhotite is not a member of the pure Fe-S system, but contains a small amount of oxygen. The monoclinic structure might be stabilized by a distortion caused by small amounts of oxygen substituting for sulfur or, alternatively, by exsolved magnetite lamellae. However, magnetization measurements by Ericsson et al. (1997) do not support the presence of exsolved magnetite.

The nature of the λ-transition is poorly understood (Schwarz and Vaughan 1972; Li and Franzen 1996). Some authors argue for a structural phase transition at 220 °C (Nakazawa and Morimoto 1971; Kissin and Scott 1982; Li and Franzen 1996), whereas others argue for a spin-ordering, electronic transition with no structural change. Differential thermal analysis (DTA) and thermodynamic calculations by Grønvold and Stølen (1992) provide no evidence for a structural transition at 220 °C, the temperature corresponding to the nC to nA structural transition of Kissin and Scott (1982). The temperature range in the KTB samples allow us to investigate the structural vs. electronic nature of the λ-transition in natural pyrrhotites.

In this paper, we describe the mineralogy and magnetic behavior of natural pyrrhotites in the KTB profiles to investigate the stability of ferrimagnetic 4C pyrrhotite and to study the nature of the λ-transition. We present a general overview on the distribution of different pyrrhotite types over the entire profile that were obtained by thermomagnetic, microanalytical, and X-ray diffraction investigations. Additionally, we discuss the relationships among lithology, mineral composition, microstructures, and magnetic properties in detail on core samples of gneisses from the depths of 564, 2325, 8080, and 9080 m. A detailed TEM analysis of pyrrhotite microstructures and superstructures is presented in a companion paper (Pósfai et al. 2000).

Analytical methods

Optical methods

Opaque phases were identified by reflected light microscopy in polished sections, using a polarizing microscope. Magnetic and non-magnetic domains in pyrrhotite were distinguished using the Bitter method (Soffel 1991) in which magnetic colloid dispersed on the surface of a polished section makes ferrimagnetic pyrrhotite appear darker. Because the magnetic particles in the colloid tend to concentrate on the domain walls, magnetic domain structures can be observed. The distribution of magnetic and non-magnetic regions in pyrrhotite grains were determined in about 400 polished sections from cores of the KTB VB (Keyssner 1992) and in about 450 polished sections from cores and cuttings of the KTB HB (Lich et al. 1992 and this work).

Electron microprobe

Analyses were made with an ARL-SEMQ electron-microprobe at the Institute of Mineralogy and Economic Geology in Aachen and with a Cameca SX51 at the Mineralogical Institute in Heidelberg. An accelerating voltage of 25 kV and a sample current of 20 nA were used. Pyrite (for Fe and S), niccolite (for Ni), and pure metals (for Co and Se) were used as standards. About 500 analyses of pyrrhotite were obtained from 30 different samples, distributed along the entire profile of the KTB VB and HB. Only analyses with totals between 98 to 102 wt% were considered for this study.

Powder X-ray diffraction

Diffraction patterns were obtained using a Siemens D5000 diffractometer with Cu$K\alpha$ radiation. The quartz 200 peak (2.128 Å) was used as an internal standard. The hexagonal pyrrhotite types produce a single, sharp, symmetrical 201 reflection at 2.065 Å; the monoclinic type displays three (Tokonami et al. 1972) or four (Morimoto et al. 1975) reflections between 2.046 and 2.069 Å. According to Tokonami et al. (1972), the 228 and 408 reflections at 2.052 Å, and the $\bar{2}28$ reflection at 2.060 Å, are about twice as intense as the $\bar{4}08$ reflection at 2.065 Å. If the intensity of the 228 reflection is significantly less than that of the 408 reflection, a mixture of monoclinic and hexagonal pyrrhotite is indicated (Arnold 1966).

Transmission electron microscopy

TEM was done using a Philips CM20-FEG instrument at the Bayerisches Geoinstitut. Details of the TEM methodology are described in the companion paper of Pósfai et al. (2000).

Magnetic measurements.

Low-field thermomagnetic susceptibility measurements [κ(T)] were performed using a CS-2 apparatus in combination with a kappabridge KLY-2 in fields of 300 A/m (Hrouda 1994). Heating and cooling rates ranged from 8 to 11 °C/min. Standard heating-cooling runs were performed in air or in argon (purity >99.998 vol%, <0.003 vol% oxygen) up to 340 °C, a temperature above the Curie point but below the onset of oxidation of pyrrhotite to magnetite. To investigate thermal stability and oxidation effects, κ(T) measurements were performed

at temperatures up to 700 °C. Analyses of the total susceptibility were made for each sample without calculation of bulk or mass susceptibility. The volume of the analyzed material ranged between 0.5 and 1 cm^3. Data processing and correction for empty furnace susceptibility were done using the software CUREVAL (Hrouda 1994).

PYRRHOTITE IN THE KTB PROFILE

The KTB boreholes were drilled into steeply inclined amphibolite-facies metamorphic rocks that are divided into three main lithologic units (Fig. 1, Duyster et al. 1995a): paragneiss (predominantly paragneisses with minor metabasite intercalations), metabasite units (amphibolite, metagabbro, and metaultramafite, with few gneiss intercalations), and variegated series (alternating paragneisses, hornblende gneisses, amphibolites, with subordinate calc-silicate and marble-bearing rocks). The typical ore-mineral assemblage in the partly graphite-bearing paragneisses consists of pyrite, pyrrhotite, chalcopyrite, sphalerite, ilmenite, and rutile; in the metabasites, the assemblage includes pyrrhotite, pyrite, chalcopyrite, ilmenite, rutile, leucoxene, and titanite (Kontny et al. 1997).

Pyrrhotite forms anhedral grains from a few micrometers to several millimeters in size, with most grains between 100 and 200 μm. Generally the amount of pyrrhotite does not exceed 1 vol% of the rock (Kontny et al. 1997). In some cases, pyrrhotite is intergrown with sphalerite (containing 10–16 mol% FeS), chalcopyrite, or both. A widespread replacement of pyrrhotite by pyrite and marcasite occurs mainly in the upper part of the profile. In contrast to the metabasic rocks with nearly randomly distributed and oriented mineralization, pyrrhotite grains in the paragneisses have a preferred distribution and orientation within the metamorphic foliation (de Wall and Worm 1993).

Profile sections

Based on ore petrography, the profile can be divided into seven sections (Fig. 1), detailed briefly below.

Section 1. Variegated and paragneiss unit, VB 0–1160 m. Pyrrhotite in the boreholes first occurs at about 220 m in the KTB VB and about 290 m in the KTB HB. The rocks above 220 m (290 m) are strongly altered, with the only Fe sulfides present being pyrite and marcasite, with a few inclusions of antiferromagnetic pyrrhotite in pyrite (Keyssner 1992). Below 220 m ferrimagnetic pyrrhotite predominates and some examples exhibit cores of antiferromagnetic pyrrhotite (Fig. 2a). Generally, this assemblage is not intergrown with pyrite.

Section 2. Metabasite rock unit, VB 1160–1610 m. Pyrrhotite occurs mostly as ferrimagnetic type with flame-like pentlandite lamellae extending into pyrrhotite.

Section 3. Paragneiss unit, VB 1610–2250 m. Antiferromagnetic pyrrhotite predominates. In the KTB HB, this section occurs in the depth interval 1530–1980 m in both variegated and paragneiss units, and thus the occurrence of antiferromagnetic pyrrhotite does not seem to be strictly lithologically controlled.

Section 4. Paragneiss and variegated unit, VB 2250–3590 m. Ferrimagnetic pyrrhotite dominates and is partially intergrown with antiferromagnetic grains. Ferrimagnetic rims around antiferromagnetic centers as well as an intergrowth of both types within a single grain were observed (Fig. 2b). Pentlandite flames and marcasite lamellae are abundant in ferrimagnetic pyrrhotite, but the latter are absent in antiferro-

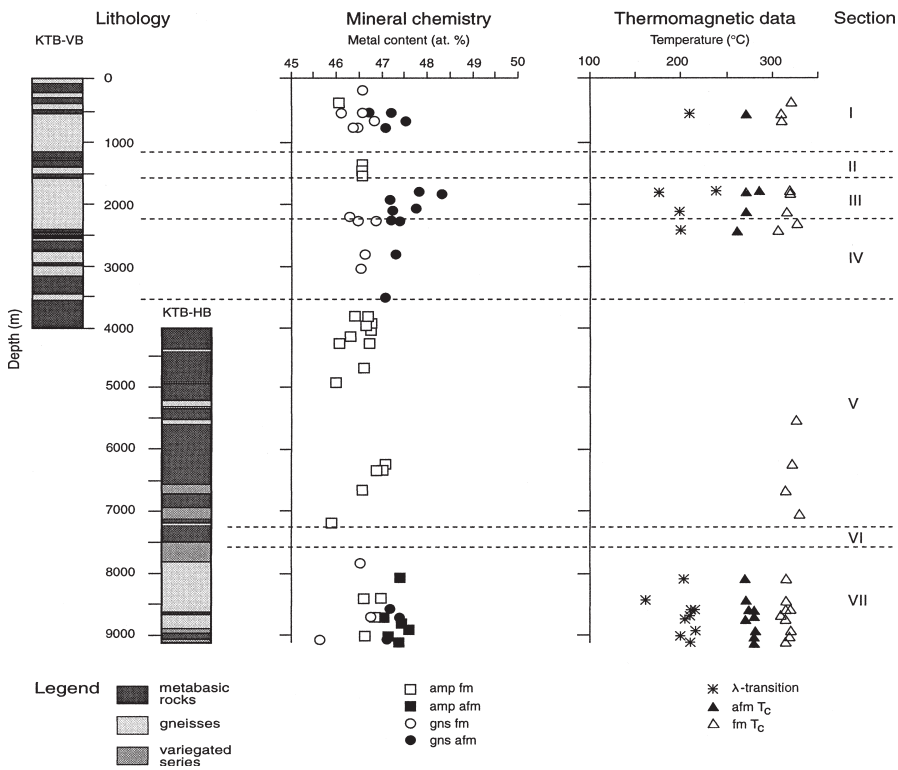

FIGURE 1. Depth-dependent distribution of different pyrrhotite types in the pilot hole (KTB-VB 0–4000 m) and the main hole (KTB-HB 4000–9101 m) with chemical composition of pyrrhotite (metal content = Fe+Ni+Co) and data from temperature-dependent magnetic susceptibility measurements ($T\lambda$: temperature of the transition of the original antiferromagnetic to a ferrimagnetic type, T_c: Curie temperatures of antiferromagnetic (afm) and ferrimagnetic (fm) pyrrhotite). Subunits I–VII are based on the distributions of ferrimagnetic Weiss-type and antiferromagnetic λ-type pyrrhotite (amp = amphibolite, gns = gneiss; for further explanation see text).

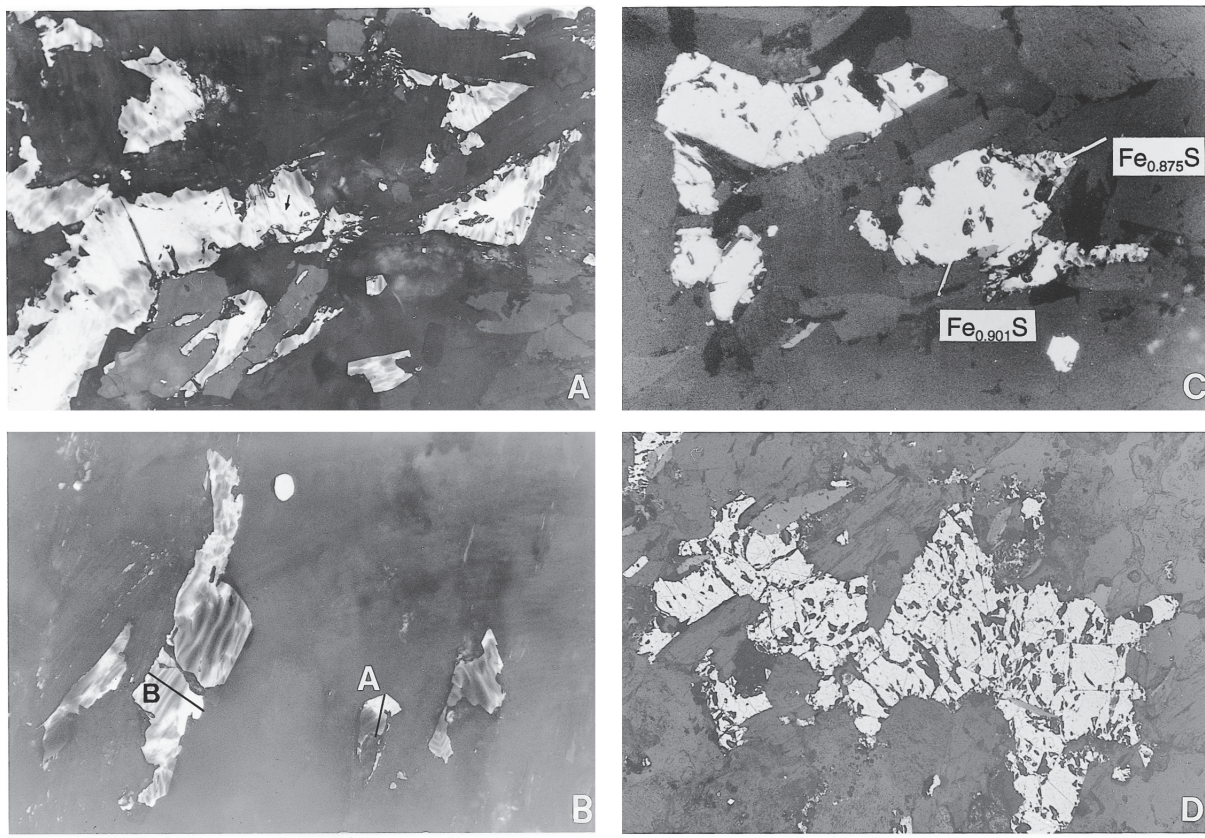

FIGURE 2. Photomicrographs of typical pyrrhotites. All in air and coated with magnetic fluid. (**a**) Pyrrhotite grains from 564 m consisting of antiferromagnetic pyrrhotite in the center and ferrimagnetic pyrrhotite at the rims. Magnetic lamellae are visible because the polished section was coated with a magnetic fluid. The arrow points to ferrimagnetic lamellae within the antiferromagnetic region. Paragneiss, KTB-VB, field of view 0.8 mm. (**b**) Mixed-type pyrrhotite from 2325 m. Lines mark the microprobe traverses (see Fig. 6). Paragneiss, KTB-VB, field of view 0.8 mm (**c**) Antiferromagnetic pyrrhotite with ferrimagnetic rims from 8080 m. The ferrimagnetic rims do not show the pronounced magnetic domain structure as in (**a**); instead, they show a diffuse accumulation of the magnetic fluid. Hornblende gneiss, KTB HB, field of view 1.4 mm. (**d**) Antiferromagnetic pyrrhotite from 9080 m. No ferrimagnetic type can be seen by optical microscopy. Amphibolite, KTB HB, field of view 0.8 mm.

magnetic pyrrhotite. Exsolution products, like lamellar magnetic domains (Keyssner 1992), occur along the basal plane of pyrrhotite.

Section 5. Metabasite rock unit, VB/HB 3590–7320 m. Ferrimagnetic pyrrhotite clearly dominates over antiferromagnetic pyrrhotite. Antiferromagnetic cores within ferrimagnetic grains were only recorded from a few specimens. This section is also characterized by minor magnetite and idioblastic pyrite, which is the major Fe sulfide down to 5400 m. Marcasite that replaces pyrrhotite disappears below 7000 m.

Section 6. Variegated unit, 7320–7660 m. Pyrrhotite is absent in this section (see details in Duyster et al. 1995b and Kontny et al. 1997).

Section 7. Variegated and paragneiss unit, 7660–9100 m. Above 8080 m (<230 °C), ferrimagnetic pyrrhotite predominates, whereas antiferromagnetic pyrrhotite becomes the main pyrrhotite phase below 8080 m. Pyrrhotite replaces pyrite with increasing depth leaving pyrrhotite pseudomorphs after pyrite. The lithological control on pyrrhotite type appears to be the inverse of that found in the upper sections. Antiferromagnetic pyrrhotite occurs with titanite in amphibolite, and ferrimagnetic pyrrhotite occurs with graphite and rutile in the gneisses. In some cases, antiferromagnetic pyrrhotite has ferrimagnetic rims without distinct lamellar magnetic domain structure (Fig. 2c). Below about 8600 m, these rims are rare (Fig. 2d).

Based on optical microscopy, and the results of microprobe, XRD, and thermomagnetic studies, two types of pyrrhotite were distinguished in the profile (Fig. 1). The general features of these two types are given below.

Ferrimagnetic pyrrhotite

XRD patterns from ferrimagnetic pyrrhotite are consistent with the 4C monoclinic superstructure of Tokonami et al. (1972), with characteristic *d*-values of 2.052, 2.060, and 2.065 Å. Electron microprobe analyses show that the Fe content ranges from 46.0 to 47.2 at% (Fig. 3). Co and Ni contents are generally below 0.1 and 0.5 at%, respectively, but concentrations of 0.5 and 1.4 at% were measured in pyrrhotite from the metabasite unit between 1160 and 1610 m in the KTB-VB, and from 4000 to 6500 m in the KTB-HB. In these rock units, pyr-

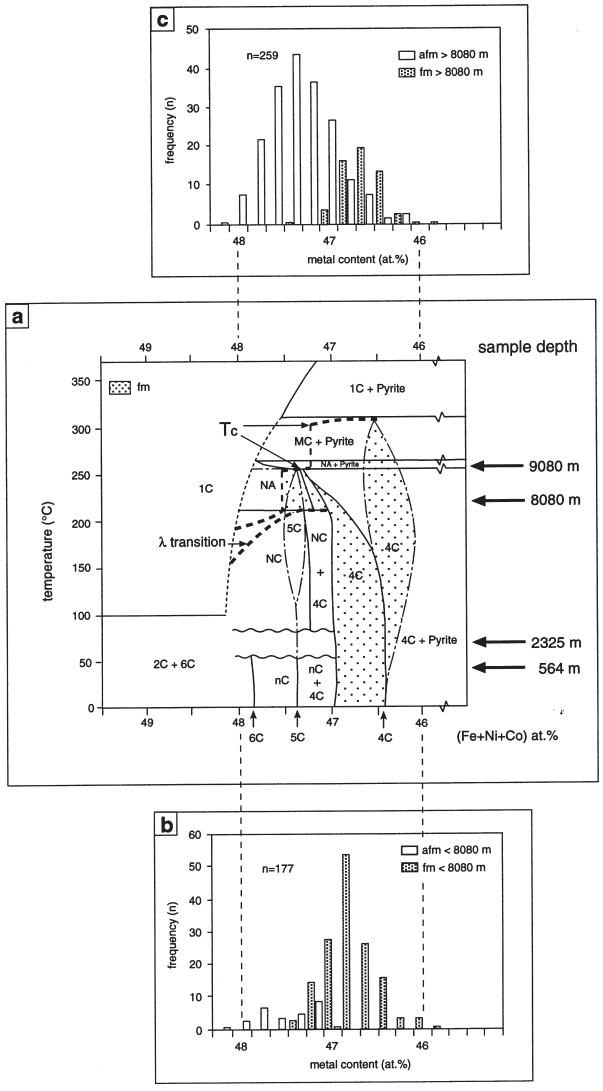

FIGURE 3. (**a**) Compilation of two different interpretations of phase relations in the Fe-S system. Solid lines: phase diagram by Kissin and Scott (1982) and Nakazawa and Morimoto (1971); dashed-dotted lines for the 5C and 4C region: after Grønvold and Stølen (1992). Magnetic phase transitions from Schwarz and Vaughan (1972) are shown in thick dashed lines. The dotted region marks the occurrence of ferrimagnetic types. (**b**) histogram of the metal contents in pyrrhotite from near surface to 8080 m depth, and (**c**) histogram of the metal contents in pyrrhotite from below 8080 m (from single microprobe analyses).

rhotite is commonly associated with Co- and Ni-rich sulfides or sulfarsenides. Ferrimagnetic pyrrhotite with metal concentrations higher than 47 at% are also present, however these samples are probably mixtures of different pyrrhotite types (Pósfai et al. 2000). The metal-poor ferrimagnetic type shows thermomagnetic Weiss-type behavior, with a T_c of 310–320 °C (Fig. 1). All $\kappa(T)$-curves of Weiss-type pyrrhotite show lower magnetic susceptibilities after the heating-cooling cycles (Fig. 4a). As no chemical reaction can be inferred from the thermomagnetic cycle, this may indicate a less degree of ferrimagnetic ordering of vacancies in the pyrrhotite lattice during cooling from T_C to room temperature.

Antiferromagnetic pyrrhotite

The XRD data from the antiferromagnetic type best fit the 5C hexagonal superstructure of Morimoto et al. (1975), with a single sharp peak at 2.067 Å that corresponds to the $10\bar{1}3$ and $20\bar{1}0$ reflections. The antiferromagnetic type generally contains 46.9 to 48.2 at% Fe, but pyrrhotite from depths greater than 8080 m shows a distinct overlap with values typical for the ferrimagnetic type (Fig. 3). XRD data for samples from below about 8080 m show a distinct dominance of the 5C hexagonal type, but with the characteristic peak shifted to a slightly higher d-value (2.070 Å) in some samples.

Thermomagnetic curves show a steep increase in susceptibility between 160 and 210 °C that reflects the so-called λ-transition from antiferro- to ferrimagnetic behavior. T_c ranges from 260 to 280 °C (Fig. 1). Most of these curves are complex and show two T_c peaks due to the presence of Weiss-type as well as λ-type pyrrhotite (Figs. 4b and 4c). The final susceptibility is always higher than the initial susceptibility as a result of pyrrhotite oxidation (discussed below). Before reaching the Curie-temperature, most thermomagnetic curves show a steep increase in susceptibility called the Hopkinson peak (Fig. 4a–4c).

PYRRHOTITE VARIATION VS. DEPTH

The occurrence of ferri- or antiferromagnetic pyrrhotite is controlled mainly by lithology only above 8080 m. Two samples from the upper and two from the lower part of the profile were studied in detail.

Pyrrhotites from 564 m and 2325 m (up to 70 °C in-situ temperature)

These samples are from gneisses of the KTB VB, which contain both ferri-and antiferromagnetic pyrrhotite (Figs. 2a and 2b).

Mineral chemistry. Pyrrhotites from 564 m are zoned (Fig. 5) with rims containing 46.0–46.5 at% Fe and 0.1–0.3 at% Ni, and cores containing 46.8–47.0 at% Fe and 0.2 at% Ni. According to Schwarz and Vaughan (1972; Fig. 3), antiferromagnetic behavior is typical for pyrrhotite with Fe contents above 47 at%. Our samples are antiferromagnetic if the sum of Fe, Ni, and Co exceeds 47% (Fig. 5b) so we present the total of Fe, Ni, and Co contents as Fe_{eq}. Keyssner (1992) found an inconsistency between magnetic behavior and composition in samples from 2000 to 3000 m, in which antiferromagnetic pyrrhotite grains have low metal contents ($Fe_{eq} < 47$ at%), similar to those of the surrounding ferrimagnetic grains. Our EMP measurements confirm the presence of low-metal ($Fe_{eq} < 46.6$ at%; Figs. 6a and 6b) and high-metal ($Fe_{eq} > 47.5$ at%; Figs. 6c and 6d) antiferromagnetic pyrrhotites.

Magnetic experiments. Temperature-dependent, low-field susceptibility measurements indicate a dominance of Weiss-type pyrrhotite with a small amount of λ-type pyrrhotite. Thermomagnetic experiments to a maximum temperature of 350 (Fig. 4b) and 700 °C (Fig. 7) reveal that λ-type pyrrhotite entirely transforms during the heating experiment to the Weiss

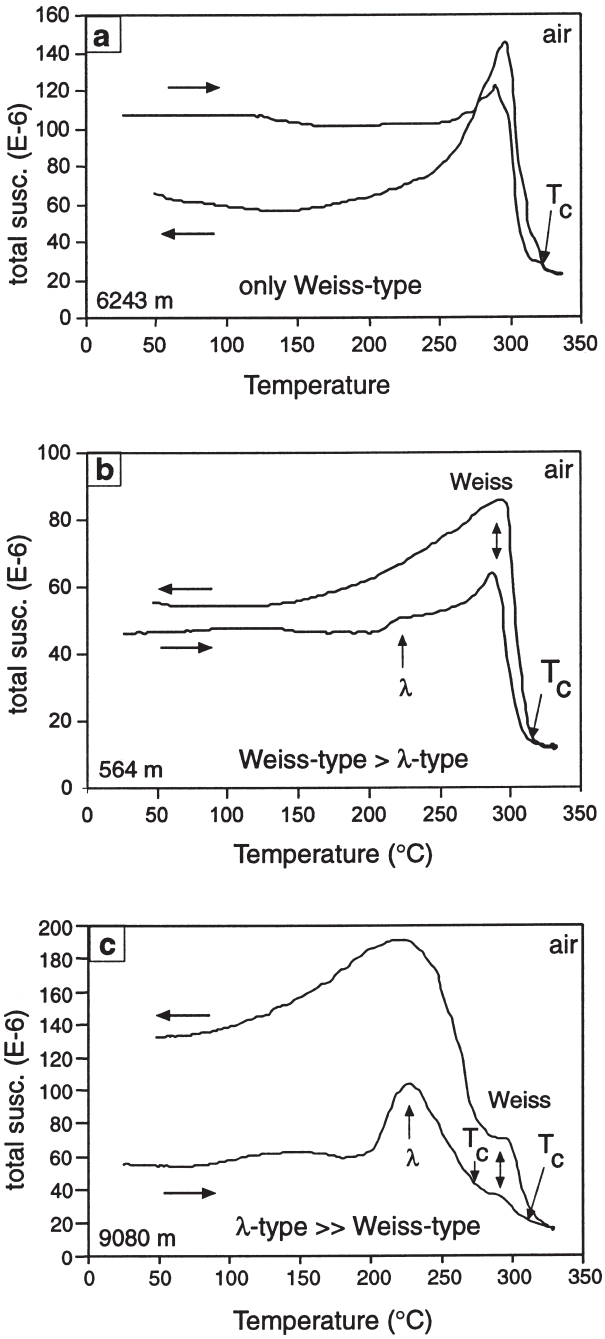

FIGURE 4. Temperature-dependent low-field susceptibility measurements of (**a**) pyrrhotite with only Weiss-type behavior, characteristic of metabasic rocks, (**b**) mixed type pyrrhotite occurring in some regions of the upper gneiss units with Weiss-type > λ-type, and (**c**) mixed types typical for the depth interval below about 8080 m with λ-type >> Weiss-type. The kinks in the susceptibility curves at 220 °C represent the λ-transition.

type. A strong increase in the final susceptibility indicates that magnetite forms at temperatures above about 350 °C, even in an Ar atmosphere.

Microstructures. TEM images and selected-area electron diffraction (SAED) patterns show that lamellar ferrimagnetic domains (Fig. 2b) commonly consist of twinned 4C pyrrhotite (Pósfai et al. 2000). Microstructural analysis of the antiferromagnetic grains in the 564 m sample (Fig. 2a) reveal wedge-shaped domains of 4C that are topotaxially intergrown with nC superstructures. Microscopic domains of 4C pyrrhotite intergrown with predominantly hexagonal superstructures may account for the locally low metal contents of antiferromagnetic cores of this sample (Fig. 5a). Optically observed ferrimagnetic lamellae within antiferromagnetic cores of grains (Fig. 2a) probably represent such intergrowths.

Pyrrhotites from 8080 m and 9080 m (220 and 260 °C in-situ temperature)

Based on the chemical and magnetic phase relations in the Fe-S system (Fig. 3), a ferrimagnetic pyrrhotite type (λ-type) should occur below 8100 m at temperatures between 220 and 260 °C. We studied solid core material from 8080 m (maximum depth from which cores were recovered) and centimeter-

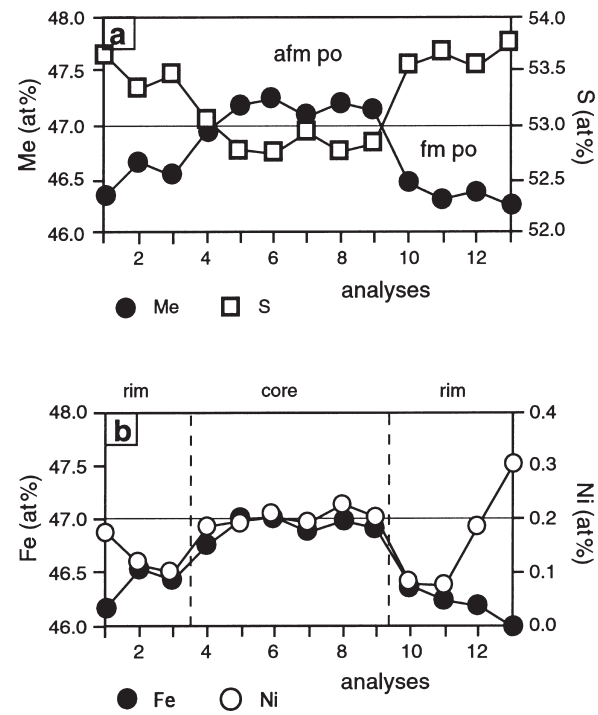

FIGURE 5. Chemical composition of zoned pyrrhotite grain from Figure 2a (sample 564 m). Distributions of (**a**) metals (Fe+Co+Ni) and sulfur, and (**b**) Fe and Ni within the antiferromagnetic core and the ferrimagnetic rim.

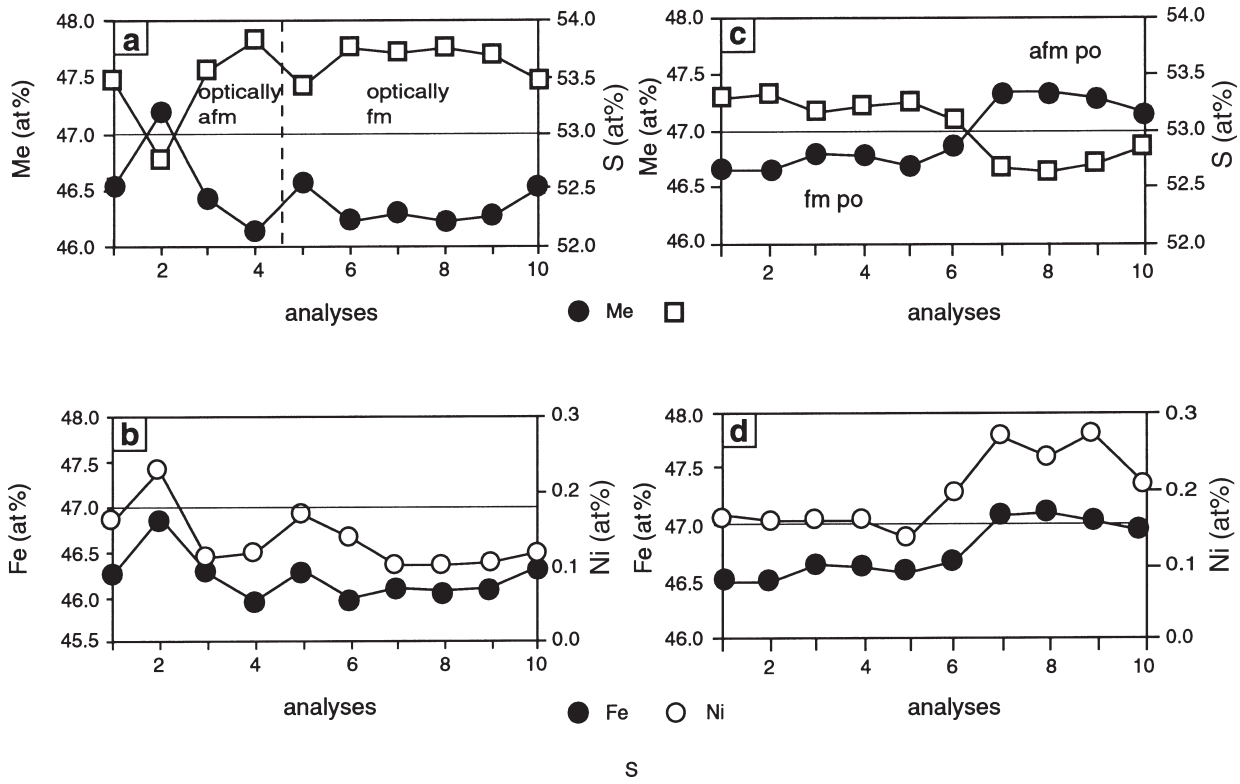

FIGURE 6. Chemical composition of antiferromagnetic (afm) and ferrimagnetic (fm) regions from pyrrhotite grains shown in Figure 2b (sample 2325 m). Distributions of (**a**) metals (Fe+Co+Ni) and sulfur, and (**b**) Fe and Ni within anomalous afm and fm type (profile A in Fig. 2b). (**c**) Metal and sulfur concentrations along profile B in Figure 2b. (**d**) Fe and Ni contents of the normal afm and fm types.

sized fragments from 9080 m. Cuttings of material from the depth interval 8080 to 9100 m were also investigated. Antiferromagnetic pyrrhotite clearly dominates (Fig. 2d), whereas a ferrimagnetic pyrrhotite occurs only as rims or small grains (<10 μm) in some samples. These ferrimagnetic grains and rims do not have the lamellar magnetic domain structure seen in other ferrimagnetic samples (Fig. 2c).

Mineral chemistry. The metal and sulfur distributions within the ferrimagnetic and antiferromagnetic types are largely similar to those in samples from 564 and 2325 m. The antiferromagnetic cores of pyrrhotite grains in sample 8080 m yield higher metal contents (Fe_{eq} = 47.40 at%) than the ferrimagnetic rims (Fe_{eq} = 46.66 at%). However, 190 single analyses from 5 different depths between 8080 and 9100 m revealed a relatively large compositional range of the antiferromagnetic type between $Fe_{eq7}S_8$ and $Fe_{eq11}S_{12}$ (Figs. 1, 3a, 8a, and 9a). Unlike other samples, there is no correlation between Fe and Ni within antiferro- and ferrimagnetic types. The Ni and Co concentrations are constant within both magnetic types (Fig. 8b), and do not change after thermomagnetic experiments where the original pyrrhotite transformed into metal-poor Weiss-type (Figs. 8d, 9d, and below).

Magnetic experiments. Thermomagnetic measurements on samples from 9080 m were performed immediately after core recovery, which took about 24 hours from the bottom of the borehole (260 °C) to the laboratory. All investigations that were conducted in the following weeks, months, and over a period of two years showed identical results. The heating curves (up to 340 °C) of all samples show λ-type behavior with minor Weiss-type contribution (Fig. 4c). A λ-shaped peak in the magnetic susceptibility curve indicates the formation and then disappearance of a ferrimagnetic modification at about 220° and 260 °C, respectively. The cooling curves reveal a distinct increase of the Weiss-type behavior (Fig. 4c) and a higher final magnetic susceptibility. This susceptibility behavior suggests that either the ferrimagnetic λ-phase does not occur at these depths, or the λ-phase has transformed into an antiferromagnetic type during the temperature and pressure decrease associated with sample recovery.

The conversion from λ- to Weiss-type pyrrhotite during heating experiments is supported by optical microscopy, as well as by chemical and XRD analyses of the heated samples. After heating to 330 °C, large antiferromagnetic grains show distinct ferrimagnetic rims, and small grains are fully transformed to ferrimagnetic pyrrhotite (similar to Fig. 2c). The composition of the antiferromagnetic type remains unchanged in the experiment, but the newly formed ferrimagnetic phase shows a composition typical for the Weiss-type pyrrhotite (Fig. 9c). The rate of transformation is influenced by the atmosphere used in the experiment. In Ar, Weiss-type behavior appears only in the cooling curves. In air there is also generally a small amount of Weiss-type material observed during heating (Figs. 10a and

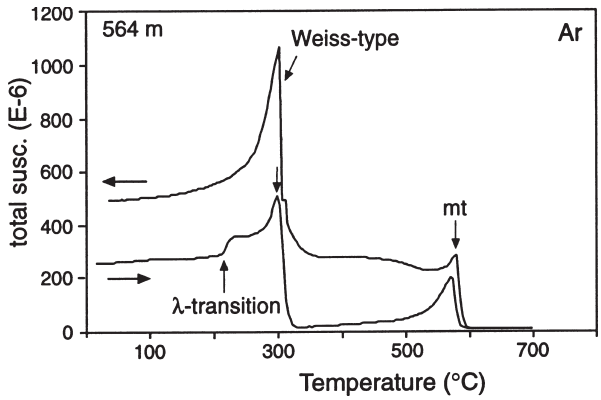

FIGURE 7. Temperature-dependent low-field susceptibility measurements up to a maximum temperature of 700 °C (sample 564 m). λ-type pyrrhotite irreversibly transforms during heating into the Weiss-type.

10b). XRD analyses reveal a clear change in peak position that is consistent with an increase of the 4C superstructure after heating (Fig. 11). These observations hold for both 8080 and 9080 m samples, and indicate a higher stability of λ-type pyrrhotite compared with λ-type pyrrhotite from less than 8080 m.

Metal-rich pyrrhotite from 8080 m that was heated to 600 °C in air, transformed completely from antiferromagnetic to ferrimagnetic pyrrhotite and magnetite (Figs. 8c and 12a). In contrast, metal-poor antiferromagnetic pyrrhotite from 9080 m showed reversible λ-type behavior in both heating and cooling segments of the thermomagnetic curve. Magnetite formed during heating in both air and Ar atmospheres (Figs. 12c and 12d). When heating the 8080 m sample to 700 °C in Ar, λ-type pyrrhotite transformed into an antiferro- or a paramagnetic phase (Fig. 12b). XRD analyses revealed a distinct shift of the 5C pyrrhotite reflection to a higher *d*-value (Fig. 11) that could be related to the 1T structure of Morimoto et al. (1975) or the 1C type. The 1T pyrrhotite is considered to be a statistical average of different nC types and has its most intense X-ray reflection ($20\bar{2}2$) at a *d*-value of 2.071 Å. The 1C type also has a

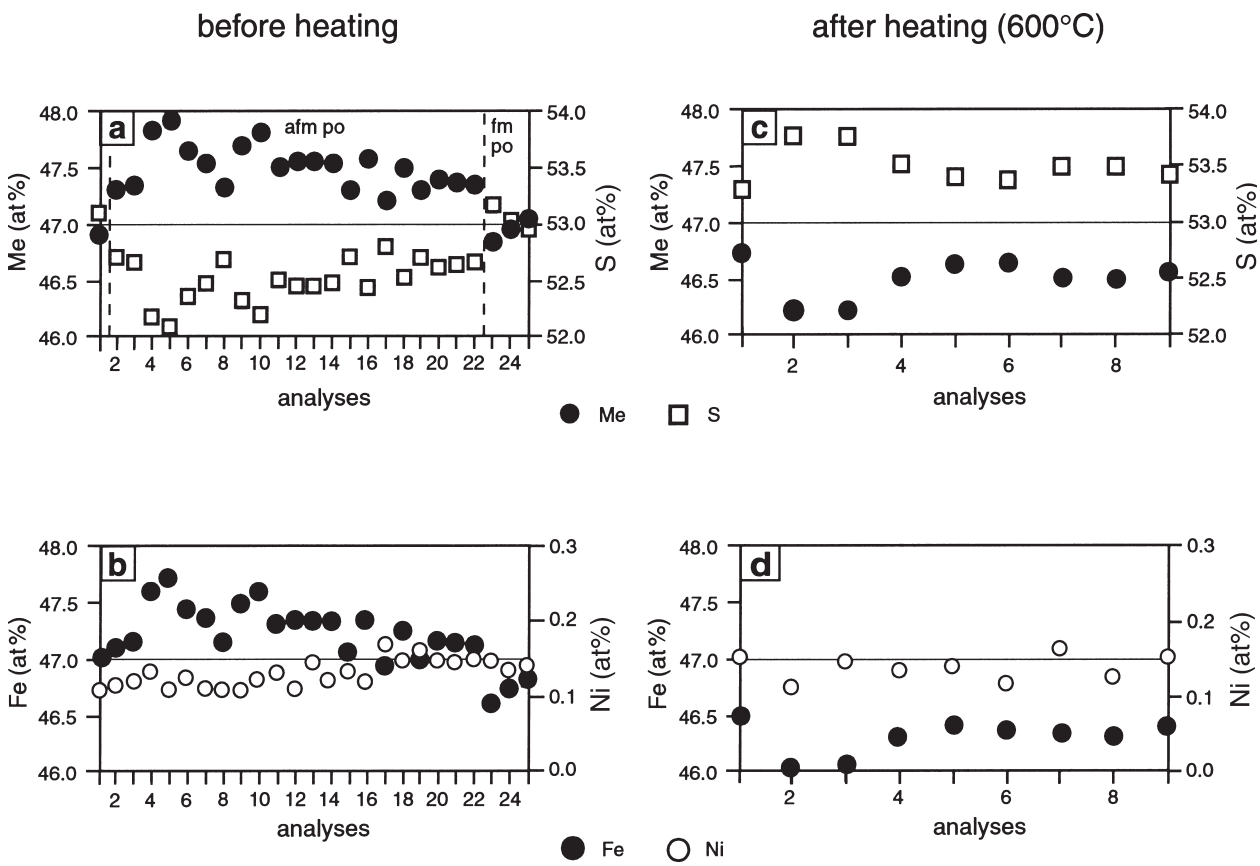

FIGURE 8. Chemical composition of antiferromagnetic pyrrhotite from 8080 m depth. (**a**) Distributions of metals (Fe+Co+Ni) and sulfur showing a metal-rich pyrrhotite. (**b**) Fe and Ni concentrations. (**c**) Metal and sulfur concentrations measured after the thermomagnetic experiment reached a maximum temperature of 600 °C (see Fig. 12a); all pyrrhotite is ferrimagnetic according to microscope observations. (**d**) The Ni concentration remains constant during this transformation.

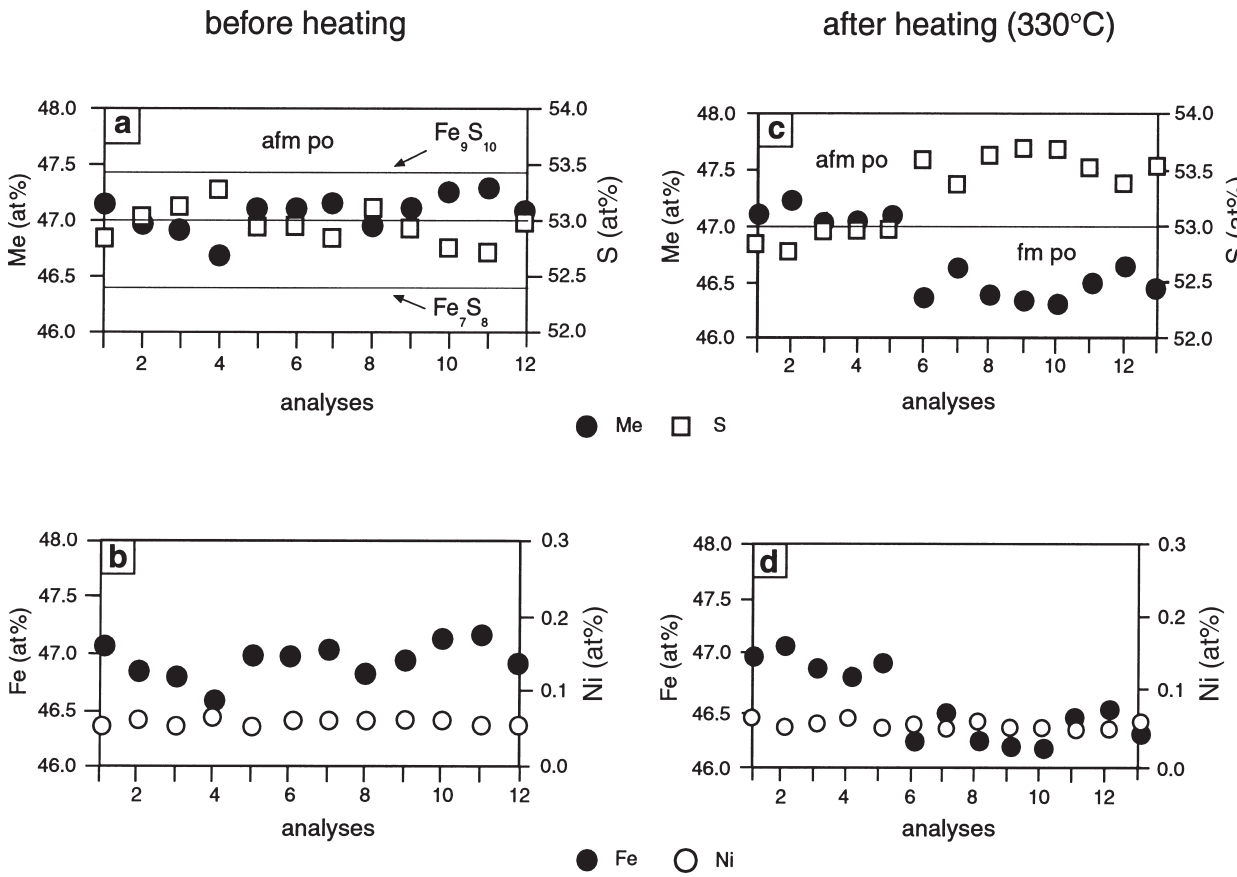

FIGURE 9. Chemical compositions of antiferromagnetic pyrrhotite from 9080 m depth. (**a**) Distribution of metals (Fe+Co+Ni) and sulfur showing a range in composition between Fe_7S_8 and Fe_9S_{10}. (**b**) Fe and Ni concentrations. (**c**) Metal and sulfur concentrations measured after the thermomagnetic experiment reached a maximum temperature of 330 °C (see Fig. 4c); the afm grains are only partially transformed to ferrimagnetic, Fe-poor pyrrhotite. (**d**) The Ni concentration is constant in both varieties.

single peak at a *d*-value of 2.07 Å (*hkl* = 102). The small additional peak at 2.093 Å is assumed to belong to the (114) reflection of troilite (Fig. 11). Troilite formation may be related to the reduction of λ-type pyrrhotite during the thermomagnetic run. Troilite formation was also observed in Ar ion-milled TEM specimens (Pósfai et al. 2000).

DISCUSSION

Ferrimagnetic Weiss-type pyrrhotite

Geophysicists accept a Curie isotherm of 310 °C for magnetic pyrrhotite (e.g., Pucher 1994). However, our findings indicate that Weiss-type pyrrhotite is a major phase within KTB rocks above depths of 8080 m, which corresponds to maximum in-situ temperature of ~220 °C. This agrees well with the stability of natural monoclinic pyrrhotite (Kullerud, 1986), but not with experimental studies of 4C stability (cf., Fig. 3a). Below 8080 m, ferrimagnetic pyrrhotite only occurs as a minor constituent and differs significantly from the Weiss-type pyrrhotite in the samples from 564 and 2325 m. Ferrimagnetic pyrrhotite from >8080 m is characterized by: (1) a lack of correlation between Fe and Ni in the different magnetic domains (Figs. 8b and 9b), and (2) a diffuse ferrimagnetic appearance without a pronounced magnetic domain structure under the magnetic colloid (Fig. 2c). In the 9080 m sample, TEM results suggest the presence of a 5C pyrrhotite with alternating filled and partially filled Fe layers that should result in ferrimagnetic behavior (see Pósfai et al. 2000). These TEM results suggest that the Weiss-type pyrrhotite is a 5C type at depths greater than 8080 m.

The transformation from antiferromagnetic, Fe-rich pyrrhotite into the ferrimagnetic, Fe-poor variety during the temperature-dependent susceptibility experiments indicates a relatively rapid transformation. A possible explanation is that the ferrimagnetic pyrrhotite from below 8080 m (>220 °C) is an artifact of quenching. Additionally, the drilling mud, which cools

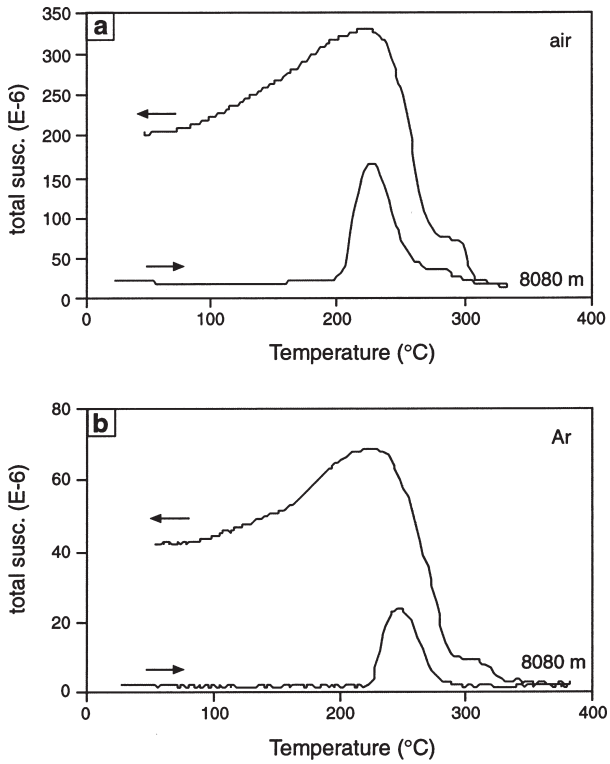

FIGURE 10. Temperature-dependent low-field susceptibility measurements of antiferromagnetic pyrrhotite from 8080 m in (**a**) air and (**b**) argon atmospheres to a maximum temperature of 380 °C.

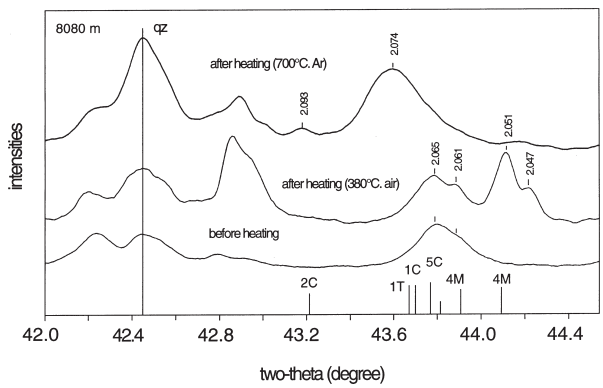

FIGURE 11. X-ray diffraction patterns of antiferromagnetic pyrrhotite from 8080 m before and after the thermomagnetic heating experiment to a temperature of 380 °C (see Fig. 10a) and 700 °C (see Fig. 12b).

and changes the redox conditions at the borehole wall, may cause an in-situ transformation from antiferromagnetic to ferrimagnetic pyrrhotite.

The combined thermomagnetic, microscopic, and XRD data document the transformation from λ- to Weiss-type pyrrhotite (Figs. 10, 11, and 12a). The phase transition changes the vacancy distribution, and an oxidation process must take place. Such a transformation may be described by the oxidation (and desulfidation) reaction $3Fe_7^{2+}Fe_2^{3+}S_{10} + 4O_2 = 3Fe_5^{2+}Fe_2^{3+}S_8 + 2Fe_3O_4 + 3S_2$. The release of sulfur explains the irreversibility of the formation of Weiss-type pyrrhotite (Fig. 12a). Antiferromagnetic relicts in ferrimagnetic pyrrhotite grains (samples 564 and 2325 m) suggest that ferrimagnetic Fe-poor pyrrhotite converted from a high-temperature pyrrhotite phase under natural conditions. The pronounced twinning seen by TEM in the ferrimagnetic type (Pósfai et al. 2000) may be a result of a phase transition from "hexagonal" type (point group 62m) into the monoclinic 4C structure (point group 2/m). Loss of the sixfold rotation axis during the transition results in six possible orientations for new 4C domains. This phase transition may be a consequence of tectonic uplift in the area (Emmermann and Lauterjung 1997).

Ferrimagnetic pyrrhotites from the KTB can have distinctly low metal concentrations (46 at%; Fig. 3). The strong depletion of Fe accompanied by an enrichment of Ni in the rims of near-surface samples (Fig. 5b) may indicate an oxidation of ferrous to ferric Fe within the outermost parts of the grains. X-ray photoelectron and Auger electron spectoscopy on natural pyrrhotite (Fe_7S_8) from the Santa Eulalia District, Mexico, showed a distinct compositional zoning with iron oxyhydroxide [FeO(OH)] in the outermost zone, and an underlying sulfur-rich zone depleted in Fe relative to the bulk of the grain (Mycroft et al. 1995). Even though the scale of these observations is smaller than ours, the oxidation mechanism could be similar.

Graham (1987) proposed that monoclinic Fe-poor pyrrhotite is not stable in the Fe-S system, but requires the presence of oxygen. According to Kullerud (1986), oxygen can enter the pyrrhotite structure in small but measurable quantities (e.g., 0.37 wt% at 500 °C, Graham et al. 1987), which raises the upper stability limit of monoclinic pyrrhotite from 260° to 310 °C. Experiments by Lusk et al. (1993) revealed that oxygen-free monoclinic pyrrhotite is not stable above 200 °C. Our temperature-dependent susceptibility measurements, done in air, showed that the formation of Fe_7S_8 + magnetite during heating is favored if some Weiss-type pyrrhotite is already present (Figs. 12a, 12c, and 12d). If no Fe_7S_8 is in the sample, λ-type pyrrhotite transforms into a paramagnetic or antiferromagnetic phase (Fig. 12b) without forming magnetite. This observation confirms that Fe-poor pyrrhotite is stabilized by oxygen.

Pyrrhotite phases within the λ-transition field

The most striking feature of the deep samples from the KTB profile (>8080 m) is the dominance of a metal-enriched pyrrhotite that is antiferromagnetic under surface conditions. The compositional range of this phase (or these phases) expands into the pyrite + pyrrhotite (4C) stability field of the phase diagram of Kissin and Scott (1982); however, pyrite does not occur in our samples (Figs. 3a and 3c). According to TEM studies (Pósfai et al. 2000), the typical structure type in the 9080 m sample is 1C that contains nC-like domains. NA and a 5C type with a composition near Fe_7S_8 are rarely observed. We did not see the 1C type in the XRD patterns. Instead, the XRD pattern is similar to that of the 5C type with intermediate Fe contents. The XRD pattern shown in Figure 11 is similar for all samples below 8080 m, and also for the 9080 m sample. Even samples with only minor antiferromagnetic pyrrhotite from above 8080 show a 5C pattern besides 4C. Only in the sample heated to

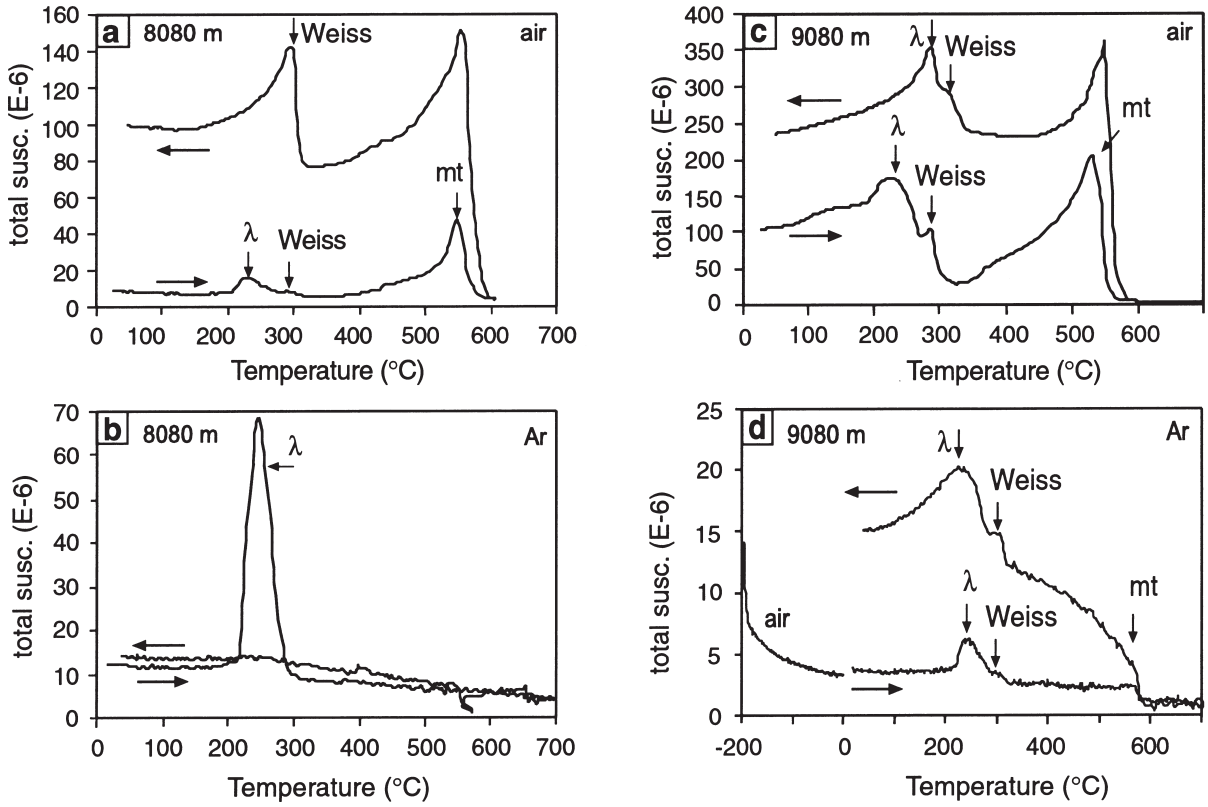

FIGURE 12. Temperature-dependent low-field susceptibility measurements to maximum temperatures of 600 and 700 °C. (**a**) In air, the antiferromagnetic, metal-rich type transforms into Weiss-type + magnetite (compare Figs. 8c and 10). (**b**) In argon atmosphere, original λ-type pyrrhotite transforms into another antiferro- or paramagnetic phase. (**c**) In air, antiferromagnetic pyrrhotite with low metal contents shows reversible λ- and Weiss-type behavior and the formation of magnetite. (**d**) In argon atmosphere, the same behavior as in air can be observed. Low-temperature (–195 to 0 °C) susceptibility measurements reveal no magnetite in the original sample.

700 °C (in an Ar atmosphere) is there a distinct shift to a lower 2θ angle, which can be related to 1C or a mixture of nC. Compared with the phase diagram of Figure 3a, these results agree with the modification of Grønvold and Stølen (1992) with the expansion of the 5C stability field in the intermediate part of the diagram to higher temperatures. However, the TEM results show that these types are not 5C but a 1C-like variety and that there are significant differences between samples from the high and low levels of the drilling with respect to the degree of ordering of vacancies (Pósfai et al. 2000). Our results show that different 5C varieties may occur in different regions of the Fe-S system.

An unusually high stability of the λ-type pyrrhotite from the deep samples is demonstrated by the reversibility of λ-type behavior in thermomagnetic experiments. This suggests that the observed antiferromagnetic superstructures were originally present in the samples (see also Pósfai et al. 2000). In contrast, antiferromagnetic pyrrhotite from near-surface samples (564 and 2325 m) shows a transition into the metal-poor Weiss-type during thermomagnetic experiments (Figs. 4b and 7) and is not as stable as in the deep samples.

In thermomagnetic data obtained from the metal-rich antiferromagnetic pyrrhotites (see Table 1 of Pósfai et al. 2000), a λ-shaped peak in the magnetic susceptibility curve indicates the formation and then disappearance of a ferrimagnetic modification at about 220 and 260 °C, respectively. It is generally accepted that the λ-transition marks the onset of the ferrimagnetic nA, 3C structure (Bennett and Graham 1980; Li and Franzen 1996). An alternative interpretation is given by Grønvold and Stølen (1992), whose DTA data showed no indication of a first-order transition in Fe_9S_{10} at 220 °C. They interpreted this temperature to correspond to a magnetic transition within the stability field of intermediate pyrrhotites and expanded the stability field of low-temperature 5C pyrrhotite to about 280 °C (see Fig. 3a).

The structural character of the 1C-like variety (disordered 1C with ordered nC-like domains) could explain the nature of the λ-transition and the unusual high stability of the λ–type pyrrhotite from the deep samples. In the heating cycles of the thermomagnetic experiments that were performed on the KTB samples, the antiferromagnetic precursors to the high-temperature λ-phase could be either the low-temperature nC varieties, or the high-temperature 1C-like phase that was preserved metastably. The conversion of nC to nA on heating was observed in situ in the TEM by Nakazawa et al. (1976). Heating of the domain-bearing, 1C-type pyrrhotite to above 220 °C would increase the degree of vacancy ordering by coarsening the domains and developing a dominance of the nA-type stacking.

Such a "gradual-ordering" transition is consistent with the DTA curves obtained by Li and Franzen (1996) that show only small anomalies associated with the λ-transition, indicating little changes in enthalpy. We suggest that within the interval of the λ-transition, the ordered nA domains grow to single domain size, resulting in a strong Hopkinson effect, which is a typical feature of thermomagnetic curves from λ-type pyrrhotites.

ACKNOWLEDGMENTS

This research was supported by the German Research Foundation (DFG) grant no. Wa 1010/1. The Bayerisches Geoinstitut funded the TEM work and two visits by M. Pósfai. We are grateful to S.D. Scott and an anonymous reviewer for their constructive comments. Special thanks are given to S. Keyssner for supplying unpublished images and rock descriptions and for his useful discussions throughout the project. We thank A. Wiechowski, R. Lang, and H.P. Meyer for assistance in electron microprobe analysis and A. Rauen for his help in the measurement of thermomagnetic curves immediately after core recovering. We are grateful to G. Friedrich for his keen interest in this work.

REFERENCES CITED

Arnold, R.G. (1966) Mixtures of hexagonal and monoclinic pyrrhotite and the measurement of the metal content of pyrrhotite by X-ray diffraction. American Mineralogist, 51, 1221–1227.

Bennett, C.E.G. and Graham, J. (1980) New observations on natural pyrrhotites. Part III. Thermomagnetic experiment. American Mineralogist, 65, 800–807.

Bertraut, E.F. (1953) Contribution a l'étude des structures lacunaires: la pyrrhotine. Acta Crystallographica, 6, 557–561.

Bosum, W., Casten, U., Fieberg, F.C., Heyde, I., and Soffel, H.C. (1997) Three-dimensional interpretation of the KTB gravity and magnetic anomaliees. Journal of Geophysical Research, 102, B8, 18,307–18,321.

Carpenter, R.H. and Desborough, G.A. (1964) Range in solid solution and structure of naturally occurring troilite and pyrrhotite. American Mineralogist, 49, 1350–1365.

de Wall, H. and Worm, H.-U. (1993) Field dependence of magnetic anisotropy in pyrrhotite: effects of texture and grain shape. Physics of the Earth and Planetary Interiors, 76, 137–149.

Duyster, J., Kontny, A., de Wall, H., and Zulauf, G. (1995a) Spät- und postvariszische Krustenstapelung am Westrand der Böhmischen Masse: Geologische Interpretation eines 9,1 km tiefen Krustenprofils. Die Geowissenschaften, 4, 135–141.

Duyster, J., Grawinkel, A., and Kontny, A. (1995b) Petrographic and Structural Characterization. in: R. Emmermann, E. Althaus, P. Giese, and B. Stöckhert, Eds., KTB Hauptbohrung, Results of Geoscientific Investigations in the KTB Field Laboratory, Final Report: 0-9101 m. KTB-Report, 95-2, B1–B80.

Emmermann, R. and Lauterjung, J. (1997) The German Continental Deep Drilling Program KTB: overview and major results. Journal of Geophysical Research, 102, B8, 18,179–18,201.

Ericsson T., Amcoff, Ö., and Nordblad, P. (1997) Superstructure formation and magnetism of synthetic selenian pyrrhotites of $Fe_7(S_{1-y}Se_y)_8$, y<1 composition. European Journal of Mineralogy, 9, 1131–1146.

Graham, J. (1987) Oxygen in pyrrhotite: 3. a mechanistic model. American Mineralogist, 72, 610–611.

Graham, J., Bennett, E.G., and van Riessen, A. (1987) Oxygen in pyrrhotite: 1. Thermomagnetic behaviour and annealing of pyrrhotites containing small quantities of oxygen. American Mineralogist, 72, 599–604.

Grønvold, F. and Stølen, S. (1992) Thermodynamics of iron sulfides, II. Heat capacity and thermodynamic properties of FeS and of $Fe_{0.875}S$ at temperatures from 298.15 K to 1000 K, of $Fe_{0.98}S$ from 298.15 K to 800 K, and of $Fe_{0.89}S$ from 298.15 K to about 650 K. Thermodynamics of formation. Journal of Chemistry and Thermodynamics, 24, 913–936.

Hrouda, F. (1994) A technique for the measurement of thermal changes of magnetic susceptibility of weakly magnetic rocks by the CS-2 apparatus and KLY-2 Kappabridge. Geophysical Journal International, 118, 604–612.

Keyssner, S. (1992) Pyrrhotin in der 4000 m tiefen Kernbohrung "KTB OBERPFALZ VB"æoptische, mineralchemische und magnetische Eigenschaften. Mitteilungen zur Mineralogie und Lagerstättenkunde, 42, 117 p. Ph.D. dissertation, RWTH Aachen.

Kissin, S.A. (1974) Phase relations in a portion of the Fe-S system. Ph.D. dissertation, University of Toronto, Canada.

Kissin, S.A. and Scott, S.D. (1982) Phase relations involving pyrrhotite below 350 °C. Economic Geology, 77, 1739–1754.

Kontny, A., Friedrich, G., Behr, H.J., de Wall, H., Horn, E.E., Möller, P., and Zulauf, G. (1997) Formation of ore minerals in metamorphic rocks of the German continental deep drilling site (KTB). Journal of Geophysical Research, 102, B8, 18,323–18,336.

Kullerud, G. (1986) Monoclinic pyrrhotite. Bulletin Geological Society of Finland, 58, Part 1, 293–305.

Lich, S., Duyster, J., Godizart, G., Keyssner, S., and de Wall, H. (1992) German Continental Deep Drilling Program (KTB)—geological survey of the Hauptbohrung 0-6000 m, KTB-Report, 92-2, B1–B83.

Li, F. and Franzen, H.F. (1996) Ordering, incommensuration, and phase transitions in Pyrrhotite. Part II: A high temperature X-ray powder diffraction and thermomagnetic study. Journal of Solid State Chemistry, 126, 108–120.

Lusk, J., Scott, S.D., and Ford, C.E. (1993) Phase relations in the Fe-Zn-S system to 5 kbars and temperatures between 325° and 150 °C. Economic Geology, 88, 1880–1903.

Morimoto, N., Gyobu, A., Mukaiyama, H., and Izawa, E. (1975) Crystallography and stability of pyrrhotites. Economic Geology, 70, 824–833.

Mycroft, J.R., Nesbitt, H.W., and Pratt, A.R. (1995) X-ray photoelectron and Auger electron spectroscopy of air-oxidized pyrrhotite: distribution of oxidized species with depth. Geochimica et Cosmochimica Acta, 59, 721–733.

Nakazawa, H. and Morimoto, N. (1971) Phase relations and superstructures of pyrrhotite, $Fe_{1-x}S$. Material Research Bulletin, 6, 345–358.

Nakazawa, H., Morimoto, N., and Watanabe, E. (1976) Direct observation of iron vacancies in polytypes of pyrrhotite. In H.-R. Wenk, Ed., Transmission electron microscopy in mineralogy, p. 304–309, Springer, New York.

Pósfai, M., Sharp, T.S., and Kontny, A. (2000) Pyrrhotite varieties from the 9.1 km deep borehole of the KTB project. American Mineralogist, 85, 1406–1415.

Pucher, R. (1994) Pyrrhotite-induced aeromagnetic anomalies in western Germany. Journal of Applied Geophysics, 32, 33–42.

Pucher, R. and Wonik, T. (1990) Eine Karte der Magnetfeldanomalien für die Umgebung der KTB-Bohrlokation in der Oberpfalz. Geologisches Jahrbuch, E44, 3–13.

Rochette, P., Fillio, G., Mattéi, J.L., and Dekkers, M.J. (1990) Magnetic transition at 30–34 Kelvin in pyrrhotite: insight into a widespread occurrence of this mineral in rocks. Earth and Planetary Science Letters, 98, 319–328.

Schwarz, E.J. and Vaughan, D.J (1972) Magnetic phase relations of pyrrhotite. Journal of Geomagnetics and Geoelectrics, 24, 441–458.

Soffel, H. Chr. (1991) Paläomagnetismus und Archäomagnetismus, 276 p., Springer Verlag.

Tokonami, M., Nishiguchi, K., and Morimoto, N. (1972) Crystal structure of a monoclinic pyrrhotite, American Mineralogist, 57, 1066–1080.

Vaughan, D.J. and Craig, J.R (1979) Mineral chemistry of metal sulfides, 493 p., Cambridge University Press.

Yund, R.A. and Hall, E.T. (1969) Hexagonal and monoclinic pyrrhotites. Economic Geology, 64, 420–423.

MANUSCRIPT RECEIVED JULY 6, 1999
MANUSCRIPT ACCEPTED APRIL 8, 2000
PAPER HANDLED BY JOHN C. SCHUMACHER